Electronic Supplementary Material (ESI) for Soft Matter.

Electronic Supplementary Information

Nonequilibrium Monte Carlo simulations of entangled polymer melts under steady shear flow

Eun Jung Roh and Chunggi Baig*

Department of Chemical Engineering, School of Energy and Chemical Engineering, Ulsan National Institute of Science and Technology (UNIST), Ulsan 44919, South Korea

*Author to whom correspondence should be addressed.

Chunggi Baig

Email: cbaig@unist.ac.kr

Phone: +82-52-217-2538

Fax: +82-52-217-2649

NEMD Method and Potential Model

Canonical (*NVT*) nonequilibrium molecular dynamics (NEMD) simulations were carried out using the well-known *p*-SLLOD algorithm[1] implemented with the Nosé-Hoover thermostat.[2,3] The set of equations of motion is given by:

$$\dot{\mathbf{r}}_i = \frac{\mathbf{p}_i}{m_i} + \mathbf{q}_i \cdot \nabla\mathbf{u}$$

$$\mathbf{p}_i = \mathbf{F}_i - \mathbf{p}_i \cdot \nabla\mathbf{u} - m_i \mathbf{q}_i \cdot \nabla\mathbf{u} \cdot \nabla\mathbf{u} - \dot{\eta}\mathbf{p}_i$$ * MERGEFORMAT

$$\dot{\eta} = \frac{p_\eta}{Q}, \quad \dot{p}_\eta = \sum_i \frac{\mathbf{p}_i^2}{m_i} - DNk_BT, \quad Q = DNk_BT\tau^2$$

(S1)

where $\mathbf{r}_i$, $\mathbf{p}_i$, and $\mathbf{F}_i$ are, respectively, the position, momentum, and force vector of the i^{th} atom of mass m_i. η and p_η are the coordinate- and momentum-like variables, respectively, of the Nosé-Hoover thermostat with the thermostat mass parameter Q. The relaxation time parameter τ was set equal to 0.24 ps for NEMD simulations. D denotes the dimensionality of the system and k_B Boltzmann's constant. N, V, and T represent the total number of atoms, the system volume, and the system temperature, respectively.

The SKS united-atom potential model[4] was adopted for GENERIC MC and NEMD simulations, except that the original rigid bond was replaced by a flexible one with a harmonic potential for NEMD. In this model, the nonbonded intermolecular and intramolecular interactions between atomic units are described by a 6-12 Lennard-Jones (LJ) potential:

$$U_{LJ} = 4\varepsilon_{ij}\left[\left(\frac{\sigma_{ij}}{r_{ij}}\right)^6 - \left(\frac{\sigma_{ij}}{r_{ij}}\right)^{12}\right]$$ * MERGEFORMAT (S2)

where $\varepsilon_{ij} = \sqrt{\varepsilon_i \varepsilon_j}$ and $\sigma_{ij} = (\sigma_i + \sigma_j)/2$ for cross interactions between atoms *i* and *j* by adopting the standard Lorentz-Berthelot mixing rules. The LJ energy parameters $\varepsilon_{\mathrm{CH_2}}/k_B$ and $\varepsilon_{\mathrm{CH_3}}/k_B$ were set equal to 47 K and 114 K, respectively, and the size parameters $\sigma_{\mathrm{CH_2}}$ and $\sigma_{\mathrm{CH_3}}$ equal to 3.93 Å identically. A cut-off distance equal to 2.5$\sigma_{\mathrm{CH_2}}$ was used in all the NEMD simulations. The intramolecular LJ interaction was active only between atoms separated by more than three bonds along the chain. The three bonded interactions [bond-stretching (U_{str}), bond-bending (U_{ben}), and bond-torsional (U_{tor}) energies] were modeled by the following expressions:

$$U_{str}(l) = \frac{k_{str}}{2}\left(l - l_{eq}\right)^2 \qquad \text{* MERGEFORMAT (S3)}$$

$$U_{ben}(\theta) = \frac{k_{ben}}{2}\left(\theta - \theta_{eq}\right)^2 \qquad \text{* MERGEFORMAT (S4)}$$

$$U_{tor}(\phi) = \sum_{m=0}^{3} a_m \cos^m \phi \qquad \text{* MERGEFORMAT (S5)}$$

where the bond-stretching constant and equilibrium bond length were k_{str}/k_B = 452,900 K/Å^2 and l_{eq} = 1.54 Å, respectively. The bond-bending constant were set as k_{ben}/k_B = 62,500 K/rad^2, and the equilibrium bending angle θ_{eq} = 114^0. The bond-torsional constants were such that (a) a_0/k_B = 1010 K, a_1/k_B = 2019 K, a_2/k_B = 136.4 K, and a_3/k_B = -3165 K. Note that ϕ = 0 represents the (most stable) *trans*-state.

Table S1 Percent acceptance rates of the MC moves (flip, end-mer rotation, reptation, concerted rotation, and end-bridging) used in the GENERIC MC simulations of the $C_{400}H_{802}$ linear polyethylene melt under shear at various flow strengths. It is particularly noticed that the acceptance rate of the end-bridging move, which is the most efficient MC algorithm driving large-scale structural deformations of the polymer systems to a steady nonequilibrium state for a given flow field, decreases significantly as the flow strength increases. This feature results in a significant increase in the computational cost of the GENERIC MC simulation for strong flow fields.

De	MC move				
	flip (%)	end-mer rotation (%)	reptation (%)	concerted rotation (%)	end-bridging (%)
0.5	78	19	9	8	0.314
1	78	19	9	8	0.277
2	78	19	9	8	0.257
10	79	19	9	9	0.113
54	79	19	9	8	0.076
108	79	19	9	8	0.066
216	79	19	9	8	0.060
540	79	19	9	8	0.050

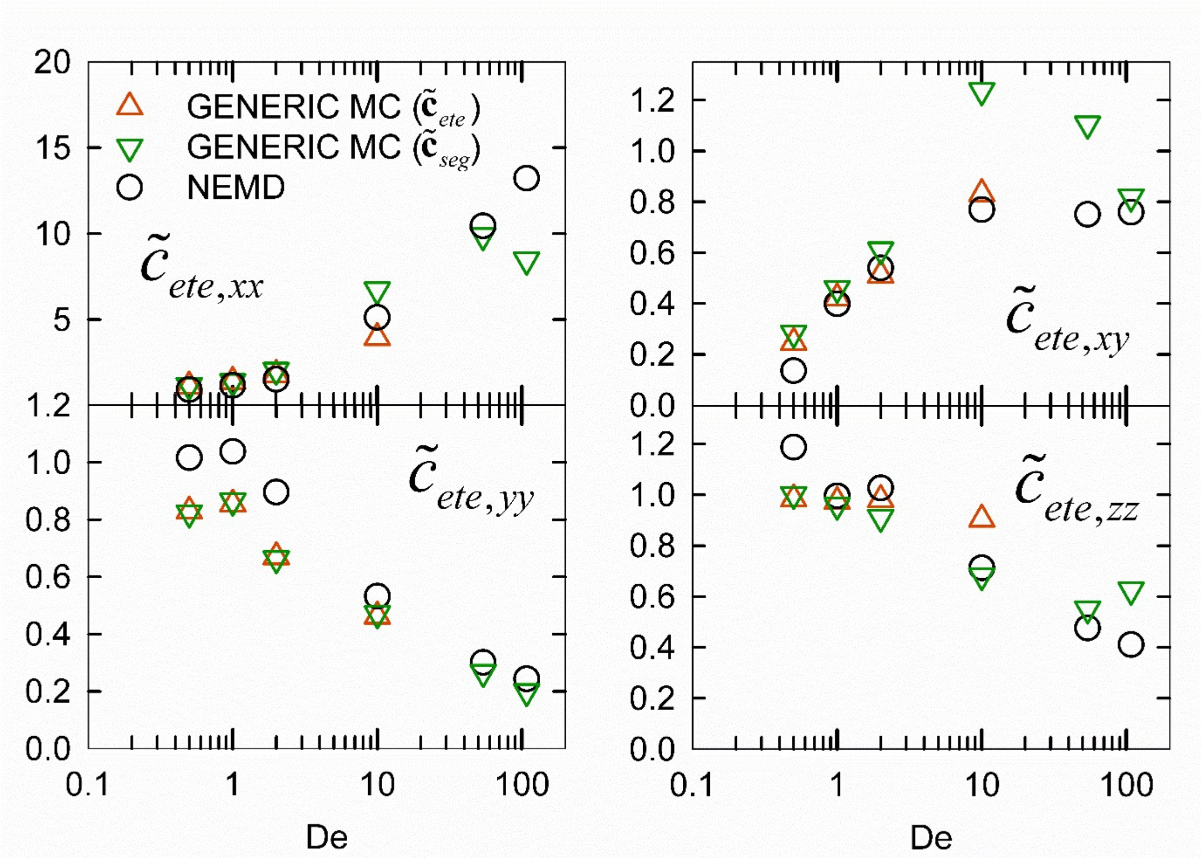

Fig. S1 Preliminary GENERIC MC results by applying the field tensor $\boldsymbol{\alpha}$ obtained from unentangled polyethylene (PE) melts[5,6] to the conformation tensor $\tilde{\mathbf{c}}_{ete}$ of the chain end-to-end vector (red triangles-up) and $\tilde{\mathbf{c}}_{seg}$ of the entanglement segment vector (green triangles-down) for the $C_{400}H_{802}$ entangled PE system in comparison with NEMD results. For the weak flow regime (De < 2), the two GENERIC results appear similar to each other with reasonable agreement with NEMD. However, systematic deviations appear as flow strength increases. For the case of $\tilde{\mathbf{c}}_{ete}$ as the structure variable, the GENERIC MC predicts a lesser degree of increasing tendency of $\tilde{c}_{ete,xx}$ and decreasing tendency of $\tilde{c}_{ete,zz}$ with increasing flow strength. For the case of $\tilde{\mathbf{c}}_{seg}$ as the structure variable, the GENERIC MC particularly overpredicts the *xy* component.

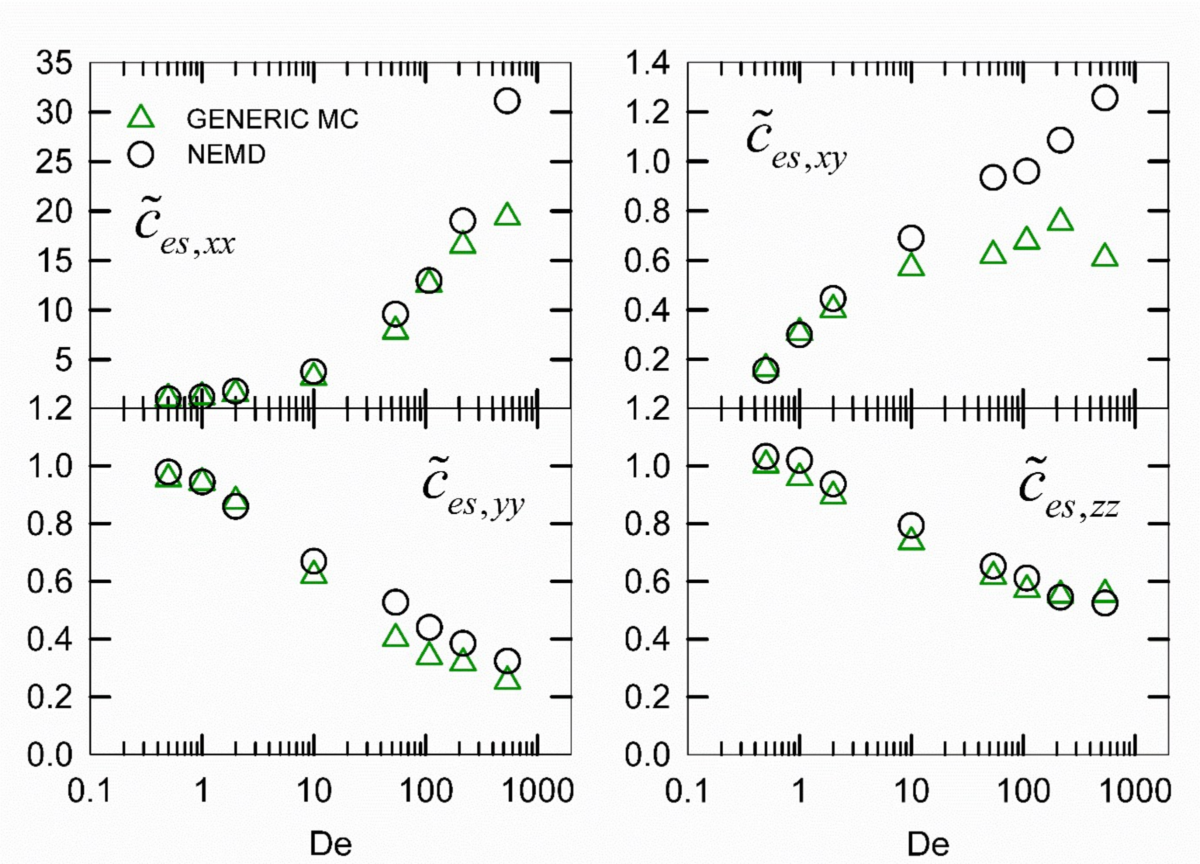

Fig. S2 Comparison between GENERIC MC (triangles) and NEMD (circles) for the *xx*, *xy*, *yy*, and *zz* components of conformation tensor &%$_{es}$ based on the entanglement strand vector (identified by the Z1-code[7,8]) as a function of De number for the simulated $C_{400}H_{802}$ entangled PE melts. This result in conjunction with that of &%$_{ete}$ (Fig. 2 in the main text) indirectly indicates that if the conformation tensor of the entanglement segment vector was chosen as the matching variable between GENERIC MC and NEMD, the conformation tensor &%$_{ete}$ of the chain end-to-end vector would not match well between the two methods.

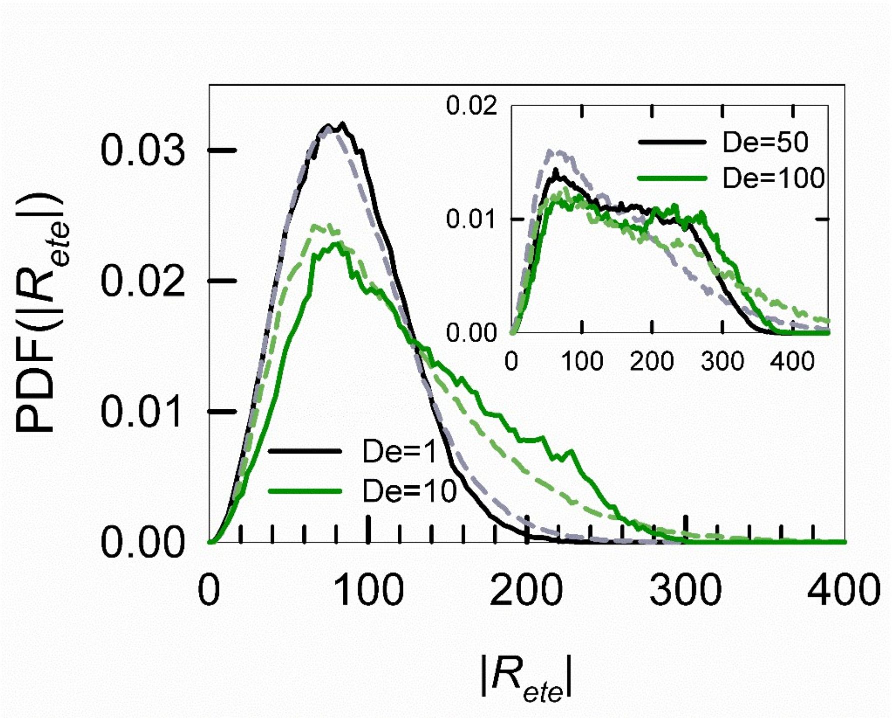

Fig. S3 Comparison between GENERIC MC (dashed lines) and NEMD (solid lines) for the probability distribution function (PDF) of the chain end-to-end distance $\left|\mathbf{R}_{ete}\right|$ at various De numbers. Note that the results of the GENERIC MC simulations involve all the chains of the system ranging from $C_{200}H_{402}$ to $C_{600}H_{1202}$. Compared to the corresponding results involving only the chains in the range $C_{350}H_{702}$ to $C_{450}H_{902}$ (Fig. 3 in the main text), the higher polydispersity leads to a broadened PDF for larger $\left|\mathbf{R}_{ete}\right|$ values, particularly noticeable for high De numbers.

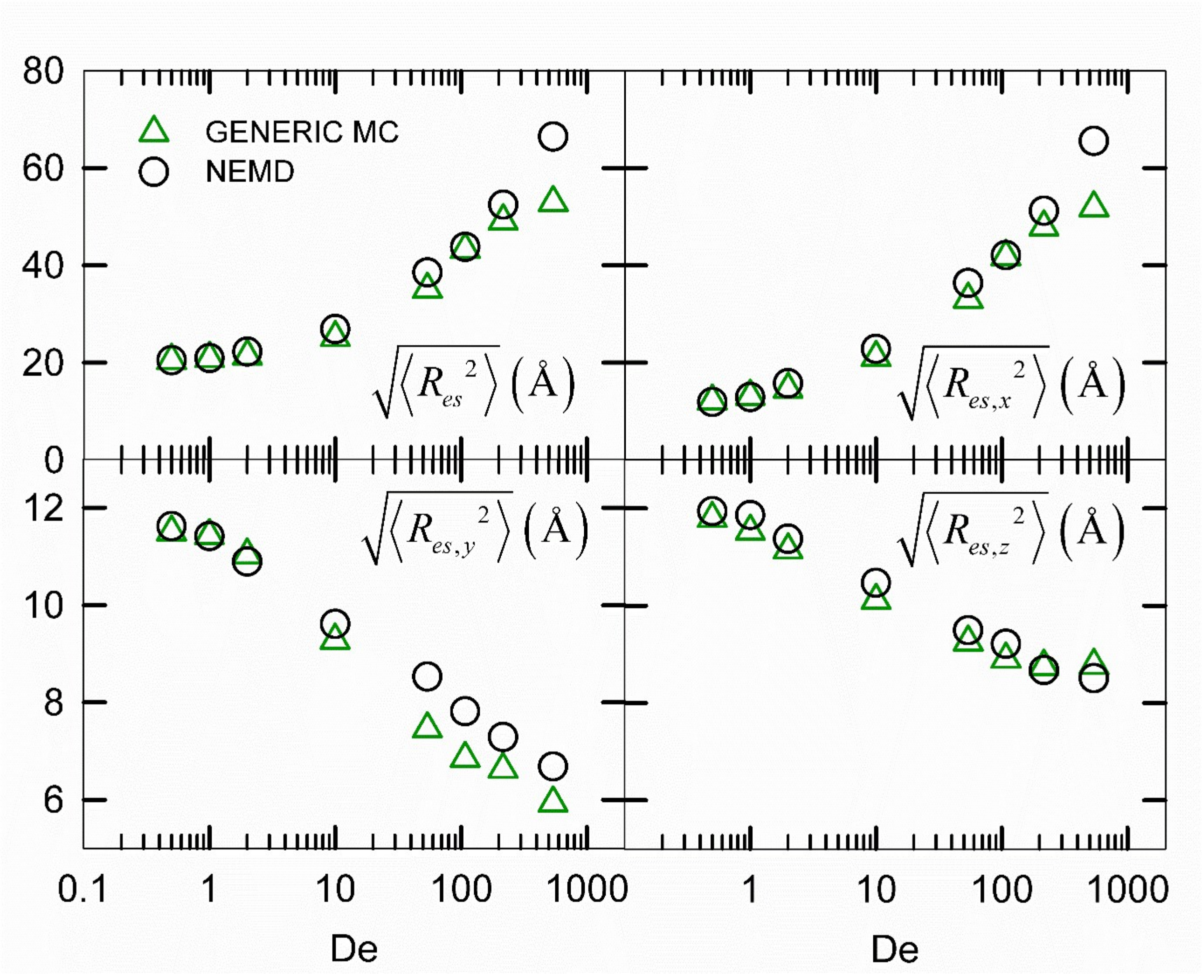

Fig. S4 Comparison between GENERIC MC (triangles) and NEMD (circles) for the mean-square distance $\sqrt{\langle R_{es}^{2}\rangle}$ and the magnitude of three (*x*, *y*, and *z*) components of the entanglement strand vector ($\mathbf{R}_{es}$) of identified by the Z1-code,[7,8] as a function of De number. As physically consistent with the chain alignment and stretch in the flow (*x*-)direction, the *x* component increases but the *y* and *z* components decrease as the shear rate increases. Additionally, the decreasing tendency of the *y* component in velocity gradient direction is stronger than that of the *z* component in neutral direction. Overall, the two simulation methods give rise to quantitatively quite similar behaviors to each other.

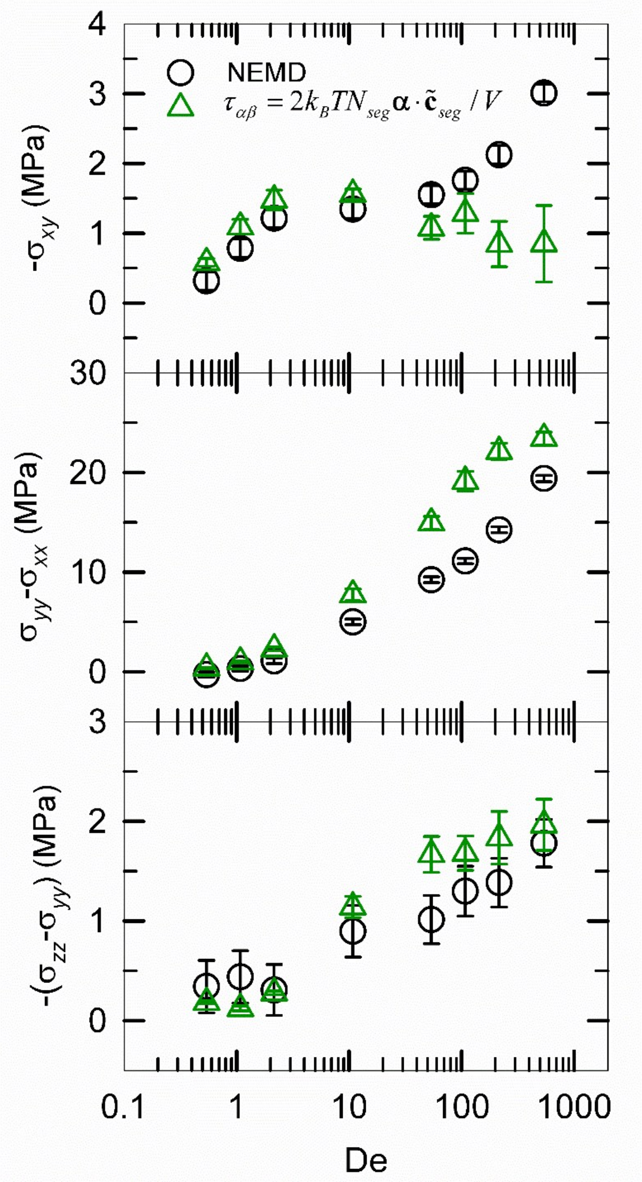

Fig. S5 Comparison of the stress tensor $\boldsymbol{\sigma}$ obtained from the NEMD simulations with the elastic stress tensor calculated based on $\tau_{\alpha\beta} = 2k_B T N_{seg} \boldsymbol{\alpha}\cdot\tilde{\mathbf{c}}_{seg} / V$ [eqn (8) in the main text] by the GENERIC MC simulations. Quantitatively consistent behaviors between the two results are observed up to De ≈ 10, beyond which systematic discrepancies appear. This is ascribed to the intrinsic inability of the GENERIC MC method to accommodate the effects of chain rotation and tumbling dynamics with structural and dynamical correlations at high shear rates.

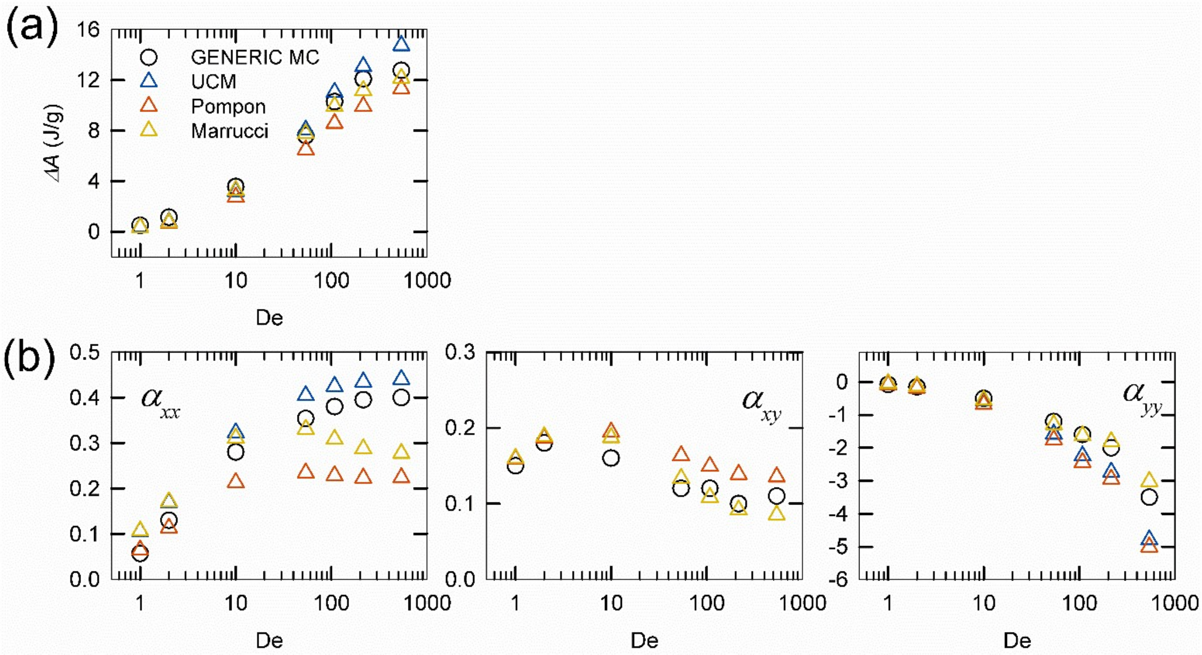

Fig. S6 Comparison for (a) the nonequilibrium Helmholtz free energy $\Delta A(\equiv A - A_{eq})$ and (b) the three (xx, xy, and yy) components of the thermodynamic force field $\boldsymbol{\alpha}$ between the GENERIC MC simulations and the three viscoelastic models [upper convected Maxwell (UCM), Pompon, and Marrucci models]. It is noted that while in the bracket[9] or GENERIC[10] formalism of nonequilibrium thermodynamics, each model is generally described as a combined set of (i) Helmholtz free energy functional with respect to structural variables (i.e., conformation tensor) and (ii) evolution equations of the structural variables in response to the flow field, the analysis here involves only (i) the free energy function with respect to the conformation tensor for which we employed the results obtained from the GENERIC MC simulations. Therefore, our preliminary result provides the information on the relevance of the functional form of free energy in terms of the structural variables assumed in each model (we leave to future work for more complete analysis with detailed numerical and theoretical comparisons). As seen in Fig. S5, the three models show qualitatively quite consistent behaviors for ΔA and $\boldsymbol{\alpha}$ in comparison with the simulation, although there appear some quantitative discrepancies. The model predictions for ΔA and α are summarized as follows:[9,10]

$$\alpha_{\alpha\beta}=\frac{1}{k_B T N_{ch} Z}\frac{\partial A}{\partial \tilde{\mathbf{c}}_{seg,\alpha\beta}}$$ where the number of entanglement segments per molecules, Z=6 for the C_{400} PE melt systems.

UCM model

$$\Delta A=\frac{1}{2}k_B T N_{ch} Z\left[\operatorname{tr}\left(\tilde{\mathbf{c}}_{seg}\right)-3-\ln\det\left(\tilde{\mathbf{c}}_{seg}\right)\right]$$
$$\alpha_{\alpha\beta}=\frac{1}{2}\left[\delta_{\alpha\beta}-\tilde{c}^{-1}_{seg,\alpha\beta}\right]$$

Pompon model

$$\Delta A=\frac{1}{2}k_B T N_{ch} Z\left[\operatorname{tr}\left(\tilde{\mathbf{c}}_{seg}\right)-3-\ln\det\left(\tilde{\mathbf{c}}_{seg}\right)-3\left(\Lambda-q\right)^2 H\left(\Lambda-q\right)\right]$$
$$\alpha_{\alpha\beta}=\frac{1}{2}\left[\frac{1}{\Lambda}\delta_{\alpha\beta}-\tilde{c}^{-1}_{seg,\alpha\beta}\right]$$

where q = 1 for linear polymers.

Marrucci model

$$\Delta A=\frac{1}{2}k_B T N_{ch} Z'\left[\operatorname{tr}\left(\tilde{\mathbf{c}}_{seg}\right)-3-\ln\det\left(\tilde{\mathbf{c}}_{seg}\right)\right]-\frac{3}{2}k_B T N_{ch} Z'_{eq}\ln\left(Z'-1\right)$$
$$\alpha_{\alpha\beta}=\frac{Z'}{2Z}\left[\delta_{\alpha\beta}-\tilde{c}^{-1}_{seg,\alpha\beta}\right]$$

where $Z'=Z\frac{\langle Z_{es}\rangle}{\langle Z_{es}\rangle_{eq}}$ (Z_{es} obtained from the Z1-code).

References

1 C. Baig, B. J. Edwards, D. J. Keffer and H. D. Cochran, *J. Chem. Phys.* 2006, **124**, 084902.

2 S. Nosé, *Mol. Phys.* 1984, **52**, 255-268.

3 W. G. Hoover, *Phys. Rev. A* 1985, **31**, 1695-1697.

4 J. I. Siepmann, S. Karaborni and B. Smit, *Nature* 1993, **365**, 330-332.

5 C. Baig and V. G. Mavrantzas, *Phys. Rev. Lett.* 2007, **99**, 257801.

6 C. Baig and V. G. Mavrantzas, *Phys. Rev. B* 2009, **79**, 144302.

7 M. Kröger, *Comput. Phys. Commun.* 2005, **168**, 209-232.

8 S. H. Jeong, J. M. Kim, J. Yoon, C. Tzoumanekas, M. Kröger and C. Baig, *Soft Matter* 2016, **12**, 3770-3786.

9 A. N. Beris and B. J. Edwards, *Thermodynamics of Flowing Systems with Internal Microstructure,* Oxford University Press, New York, 1994.

10 H. C. Öttinger, *Beyond Equilibrium Thermodynamics,* John Wiley & Sons, New Jersey, 2005.